Chinese Chemical Letters 35 (2024) 109147

Contents lists available at ScienceDirect

Chinese Chemical Letters

journal homepage: www.elsevier.com/locate/cclet

Defect engineered electrocatalysts for C–N coupling reactions toward urea synthesis

Shengkai Li[a,b], Yuqin Zou[b], Chen Chen[b], Shuangyin Wang[b,*], Zhao-Qing Liu[a,*]

[a] Guangzhou Key Laboratory for Clean Energy and Materials/Key Laboratory for Water Quality and Conservation of the Pearl River Delta, Ministry of Education, Guangzhou University, Guangzhou 510006, China
[b] State Key Laboratory of Chemo/Bio-Sensing and Chemometrics, College of Chemistry and Chemical Engineering, Advanced Catalytic Engineering Research Center of the Ministry of Education, Hunan University, Changsha 410082, China

ARTICLE INFO

Article history:
Received 15 August 2023
Revised 4 September 2023
Accepted 25 September 2023
Available online 27 September 2023

Keywords:
Electrocatalysis
Defective electrocatalyst
Co-reduction
C–N coupling
Urea synthesis

ABSTRACT

Urea is extensively used in agriculture and chemical industry, and it is produced on an industrial scale from CO_2 and Haber–Bosch NH_3 under relatively high temperature and high pressure conditions, which demands high energy input and generates masses of carbon footprint. The conversion of CO_2 and N sources (such as NO_2^-, NO_3^-, and N_2) through electrocatalytic reactions under ambient conditions is a promising alternative to realize efficient urea synthesis. Of note, the design of electrocatalyst is one of the key factors that can improve the efficiency and selectivity of C–N coupling reactions. Defect engineering is an intriguing strategy for regulating the electronic structure and charge density of electrocatalysts, which endows electrocatalysts with excellent physicochemical properties and optimized adsorption energy of the reaction intermediates to reduce the kinetic barriers. In this minireview, recent advances of defect engineered electrocatalysts in urea electrosynthesis from CO_2 and various N reactants are firstly introduced. Mechanistic discussions of C–N coupling in these advances are presented, with the aim of directing future investigations on improving the urea yield. Finally, the prospects and challenges of defect engineered electrocatalysts for urea synthesis are discussed. This overview is expected to provide in-depth understanding of structure–reactivity relationship and shed light on future electrocatalytic C–N coupling reactions.

1. Introduction

Organonitrogen compounds such as amides, amines and urea, are widely used to manufacture fine chemicals, pharmaceutical intermediates, agrochemicals and fertilizers [1–3]. Organonitrogen compounds conventionally originate from the reaction between C and N sources under harsh reaction conditions, thus aggravating the energy crisis and environmental concerns [4–6]. Undoubtedly, energy-saving and environmentally friendly synthetic method is urgently required to replace traditional methods.

N-integrated electrocatalytic CO_2 reduction strategies for organonitrogen compounds synthesis have some notable benefits compared with the current industrial routes. First, electrocatalytic method is a clean and sustainable synthetic route occurs in which hazardous redox reagents are replaced by an electricity [7–9]. Most of the electrocatalysts work under room temperature and standard pressure conditions, thus electrocatalytic reaction is easy to control. Second, CO_2 is used as the C source in these reactions, which could meet the demands of carbon neutrality [10–12]. Third, other N sources aside from NH_3 can be used, such as NO, NO_2^-, NO_3^-, and N_2 [13–15]. Currently, over half of global NH_3 production is consumed in the synthesis of organonitrogen compounds, and NH_3 is typically produced *via* the energy-intensive and fossil-fuel based Haber–Bosch process [16–18].

Urea, a typical organonitrogen compound, is extensively used in agriculture and chemical industry [19,20]. Urea is produced on an industrial scale from CO_2 and Haber–Bosch NH_3 under relatively high temperature and high pressure conditions, which demands high energy input and generates masses of carbon footprint [6,21]. In the past decades, the synthesis of urea from CO_2 through relatively mild electrochemical reactions has aroused extensive attention [11–13,22]. Great efforts have been made to improve the efficiency and selectivity of C–N coupling reactions toward urea synthesis, but the reaction rates and energy utilization efficiencies are unsatisfactory, and the reaction selectivity is also hindered by the diverse reaction pathways and complex reaction mechanisms

* Corresponding authors.
E-mail addresses: shuangyinwang@hnu.edu.cn (S. Wang), lzqgzu@gzhu.edu.cn (Z.-Q. Liu).

https://doi.org/10.1016/j.cclet.2023.109147
1001-8417/

[23,24]. In spite of that, researchers have never stopped to pursuing more efficient urea synthesis, especially the design of electrocatalysts.

According to the second law of thermodynamics, it is not hard to know that defects extensively exist in nanomaterials [25–27]. Defects can modulate the distribution of the electronic structure and disturb the periodic crystal structure of nanomaterials, thereby enhancing the electrocatalytic reaction activity by precise control of the species, concentration and location [28–30]. In recent years, various defect engineered electrocatalysts have developed for improved electrocatalytic synthesis of urea, and some typical examples have been mentioned upon in several recent reviews [11–13,22]. A more comprehensive understanding of defective electrocatalysts in terms of their intrinsic properties, catalytic mechanisms, and interface reaction processes is essential to identify the relationship between the defect sites and electrocatalytic reaction activity, facilitating the preparation of electrocatalysts for effective synthesis of urea.

2. Defective engineered electrocatalysts for urea synthesis

The "one-step" conversion of C and N sources *via* electrocatalytic reactions under ambient conditions is a promising alternative to complex industrial method for efficient urea synthesis. In recent years, a series of robust electrocatalysts have been developed for electrocatalytic coupling of CO_2 and NO_2^-/NO_3^- or N_2 into urea [10–12,23]. Numerous works proved the defects in electrocatalysts could significantly enhance the electrocatalytic reaction activity [27,30,31], hence defective engineered electrocatalytic C–N coupling reactions for urea synthesis have aroused enormous interests. Herein, defective engineered electrocatalysts for urea synthesis under ambient conditions *via* the electrocatalytic coupling of CO_2 and NO_2^-/NO_3^- or N_2 will be discussed in detail.

2.1. C–N coupling of CO_2 and NO_2^-/NO_3^- for urea synthesis

Human activities discharge plenty of nitrogen-containing substances into surface water in the form of NO_2^-/NO_3^-, posing severe risks to public health. Traditional catalytic conversion of harmful NO_2^-/NO_3^- into harmless nitrogen molecules fails to realize the product upgrading and the maximum use of energy and resources. Recent studies indicate the electrocatalytic coupling of CO_2 and NO_2^-/NO_3^- into urea is an ideal alternative, which simultaneously realize the utilization of CO_2, control of water pollution and acquirement of high value-added products.

In the early stages, Furuya *et al.* [32,33] used Ni-phthalocyanine (Ni-Pc) electrocatalysts for simultaneous reduction of CO_2 and NO_2^- to produce urea, an optimal current efficiency of 40% was obtained at −1.5 V *vs.* standard hydrogen electrode (SHE), but the complex reaction pathways of CO_2 reduction reaction (CO_2RR) allowed very few active species to combine with N-containing intermediates to complete the C–N coupling reaction, and the competitive hydrogen evolution reaction (HER) also limits the reaction efficiency. Subsequent studies have shown that some transition metal oxides and p-block-elements based electrocatalysts can be candidates for this reaction because their inherent weak H adsorption abilities can restrain the HER [22,34]. Especially, inspired by the defect engineering strategy, a series of robust defective electrocatalysts have been developed to simultaneously activate N- and C-containing intermediates and reduce the HER for more effective urea synthesis.

Cao *et al.* [35] designed O vacancy (V_O)-riched Cu-doped anatase TiO_2 nanotubes catalysts (Cu–TiO_2) to improve the electrocatalytic co-reduction of CO_2 and NO_2^-. A little red shift of (101) plane was observed in Cu–TiO_2, indicating Cu doping reduced the TiO_2 lattice constant (Fig. 1A). The remarkably increase in Ti^{3+}/Ti^{4+} ratio indicated Cu doping contributed to the occurrence of V_O on Cu–TiO_2 (Fig. 1B). The V_O facilitated the adsorption and activation of NO_2^- and cooperated with high CO_2RR active Cu sites to realize efficient urea synthesis, and a Faraday efficiency (FE) of 43.1% was obtained at a low overpotential of −0.4 V *vs.* reversible hydrogen electrode (RHE) (Fig. 1C). The potentials mentioned in this work are relative to RHE, unless otherwise stated. Meng *et al.* [36] found V_O–ZnO porous nanosheets display an excellent performance in electrocatalytic synthesis of urea from CO_2 and NO_2^-. The experimental results indicated CO_2 and NO_2^- filled the surface vacancy for accelerating urea synthesis, and the V_O–ZnO displays a ∼3- and 2-fold enhancement of the FE_{urea} and urea yield rate (r_{urea}), respectively, compared with that of pure ZnO at an applied potential of −0.79 V (Figs. 1D and E). Lv *et al.* [37] reported the intriguing electrocatalytic urea synthesis process on a defect engineered indium oxyhydroxide catalyst with V_O (V_O–InOOH) using CO_2 and NO_3^- as reactants. V_O–InOOH exhibited much better performance compared with pristine InOOH in terms of both urea yield (592.5 *vs.* 378.4 μg h^{-1} $mg_{cat.}^{-1}$) and FE_{urea} (51.0% *vs.* 26.3%), indicating the presence of V_O resulted in the improvement of C–N coupling efficiency. Wei *et al.* [38] used the V_O-riched CeO_2 (V_O–CeO_2) as the electrocatalyst for urea synthesis with CO_2 and NO_3^- as reactants. Experimental results indicated the urea production was tightly associated with the V_O concentration, and CeO_2 treated with 750 °C (V_O–CeO_2-750), the one had the highest V_O contents (Fig. 1F), exhibited the highest urea yield of 943.6 mg h^{-1} g^{-1} at −1.66 V, which was almost three times as much as that of pristine CeO_2 (Fig. 1G). Beside to metal-based electrocatalysts, a novel metal-free F-riched carbon nanotubes (F-NCT) electrocatalyst was developed for urea synthesis with CO_2 and NO_3^- as reactants by Liu *et al.* [39]. The F-doping introduced lots of defects in CNT according to the Raman spectra (Fig. 1H), and a high r_{urea} of 6.36 mmol h^{-1} g^{-1} with a corresponding FE_{urea} of 18.0% was achieved for F-CNT catalyst mediated urea synthesis at –0.65 V (Fig. 1I). The r_{urea} was 3.8 times as high as that obtained from CNT catalyzed urea synthesis, proving the defects introduced by F doping facilitate the C–N coupling reaction to form urea. Recently, Li *et al.* [40] integrated facet and defect engineering strategy to develop a highly efficient V_O-rich indium hydroxide nanocube catalyst with dominant facets (denoted as V_O-S-IO-6) for urea synthesis from the electrocatalytic co-reductive coupling of NO_3^- and CO_2. The In 3d orbital of V_O-S-IO-6 shifted to lower binding energy compared with M-IO and S-IO, implying the increase of the local electron density of In caused by delocalized electrons after oxygen escaping (Fig. 1J). Linear cyclic scanning (LSV) measurements proved V_O-S-IO-6 had the best performance toward electrocatalytic co-reduction of NO_3^- and CO_2 (Fig. 1K), and a high r_{urea} of 910.4 μg h^{-1} mg^{-1} and FE_{urea} of 60.6% was achieved at −0.6 V (Fig. 1L), indicating the introduction of V_O contributed to the C–N coupling toward urea synthesis.

2.2. C–N coupling of CO_2 and N_2 for urea synthesis

N_2 is the most abundant and cheapest N source on the earth, and the report on electrocatalytic N_2 reduction to NH_3 inspired researchers to synthesize urea in N_2-integrated electrocatalytic CO_2 reduction in spite of the inertness and high bonding energy of the N≡N bonds [41,42]. Compared with the NO_2^-/NO_3^--integrated electrocatalytic CO_2 reduction for urea synthesis, the N_2-integrated electrocatalytic CO_2 reduction one not only lowers the cost of raw material but also circumvents the use of energy-intensive fossil-fuel [10–12].

Kayan *et al.* [43] firstly used aqueous solution as the proton source to explore the co-reduction of N_2 and CO_2 for the production of urea on a polypyrrole-coated Pt electrode under a mixed atmosphere of 30 bar N_2 and 30 bar CO_2, and an optimized urea formation rate of 31.8 μg h^{-1} cm^{-2} and of FE_{urea} of 6.9% at −0.325 V

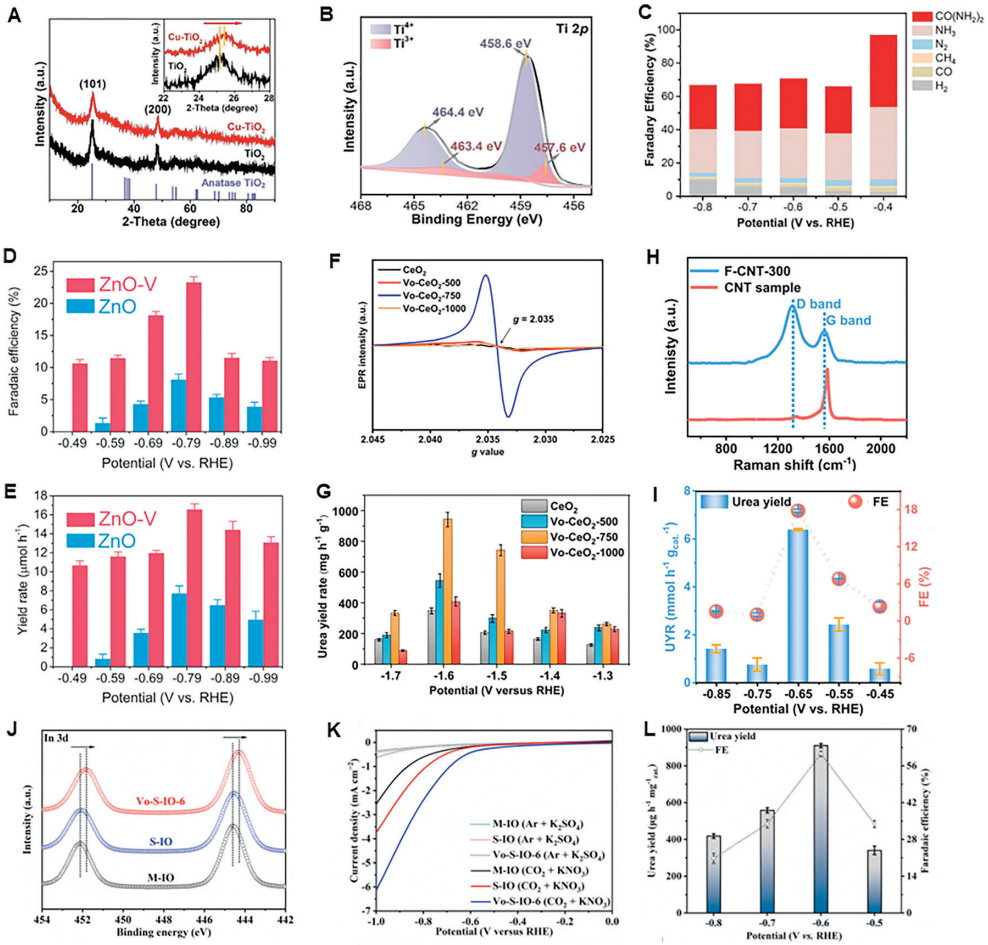

Fig. 1. Defective electrocatalysts mediated coupling of CO_2 and NO_2^-/NO_3^- for urea synthesis. (A) XRD patterns of Cu–TiO_2 and TiO_2; (B) XPS spectra of Ti 2p orbital on Cu–TiO_2. (C) FE of the urea synthesis on Cu–TiO_2. (A–C) Reproduced with permission [35]. Copyright 2020, Elsevier Inc. (D) FE_{urea} and (E) r_{urea} under the given potentials over ZnO-V. (D, E) Reproduced with permission [36]. Copyright 2021, Cell Press. (F) EPR spectra CeO_2, V_O-CeO_2-500, V_O-CeO_2-750, and V_O-CeO_2-1000. (G) r_{urea} of CeO_2, V_O-CeO_2-500, V_O-CeO_2-750, and V_O-CeO_2-1000 at various applied potentials. (F, G) Reproduced with permission [38]. Copyright 2022, American Chemical Society. (H) Raman spectra of F-CNT-300 and CNT sample. (I) Urea yield rates and FE values at different potentials for F-CNT-300 in CO_2 saturated 0.1 mol/L KNO_3 electrolyte with CO_2 flow. (H, I) Reproduced with permission [39]. Copyright 2022, Elsevier Inc. (J) In 3d XPS spectra of M-IO, S-IO, and V_O-S-IO-6. (K) LSV curves recorded on the M-IO, S-IO, and V_O-S-IO-6 during urea electrosynthesis and the electroreduction of V_O-S-IO-6 in electrolyte without NO_3^- or CO_2. (L) Yields and FEs of urea during urea electrosynthesis with V_O-S-IO-6 catalyst at different potentials after collecting –7.65 C of charge. (J–L) Reproduced with permission [40]. Copyright 2023, Elsevier Inc.

vs. NHE were achieved. The replace of ambient working condition to high pressure one favors to save energy and minimize the requirement of synthesis equipment. Inspired by the fact that metal alloying and defect engineering can promote the electronic interactions and provide more active sites for electrocatalytic reaction [44–47]. Wang's group [48] developed the electrocatalyst of PdCu alloy nanoparticles on V_O-riched defective TiO_2 nanosheets (Pd_1Cu_1/TiO_2–V_O) for the efficient electrocatalytic synthesis of urea *via* the coupling of N_2 with CO_2 under ambient conditions. The interaction between TiO_2–V_O-400 (TiO_2 with treatment at 400 °C) with the most abundant defect sites and PdCu alloy was verified by X-ray photoelectron spectroscopy (XPS) analysis (Figs. 2A and B). The temperature programmed desorption (TPD) spectra illustrated that the proposed electrocatalyst displayed a stronger chemical adsorption ability for CO_2 and N_2 due to the strong electronic interaction between the bimetal alloys and the TiO_2-V_O-400 (Fig. 2C). *Operando* synchrotron radiation–Fourier transform infrared spectroscopy (SR–FTIR) analysis proved the formation of urea (Figs. 2D and E), and a desirable r_{urea} of 3.36 mmol g^{-1} h^{-1} and FE of 8.92% at –0.4 V were obtained (Figs. 2F and G). Also, higher r_{urea} and FE_{urea} of Pd_1Cu_1/TiO_2-V_O-400 than that of Pd_1Cu_1/TiO_2-V_O were identified. On the basis of this work, Pan *et al.* [49] further found Pd_1Cu_1/TiO_2-V_O had better performance than Pd_1/TiO_2-V_O on electrocatalytic co-reduction of N_2 and CO_2 for urea synthesis, indicating the important role of dual-atom Pd_1Cu_1 site. Wu *et al.* [50] reported the defective bimetallic Cu–Bi catalyst for urea electrosynthesis. HR-TEM images showed the bimetallic Cu–Bi had ordered regions consisting of missing-atom defects (Fig. 2H), and the EPR analysis also proved the presence of higher concentration of unsaturated Bi sites with unpaired electrons (Fig. 2I). Significantly, defective Cu–Bi catalyst offered a maximum urea concentration of 0.45 ± 0.06 mg/L and the largest faradaic efficiency of 8.7% ± 1.7% at −0.4 V (Fig. 2J), and meanwhile, it exhibited much higher active in producing urea compared with monometallic (Cu and Bi) and bimetallic (Cu–Bi mixture and intact Cu–Bi) catalysts (Fig. 2K). This work provides insights into intriguing relationships between defective structure and catalytic activity, shedding light on the rational design of defective electrocatalysts for producing urea from N_2 and CO_2 molecules.

N_2-integrated electrocatalytic CO_2 reduction for urea synthesis has huge application prospects, but the exceedingly sluggish kinetics of N_2 reduction limits the overall rate of urea production [11,12,22]. Current works indicate the r_{urea} and FE_{urea} are unsatisfactory (Table 1) [2,23,35–40,48–70]. Of note, current works about

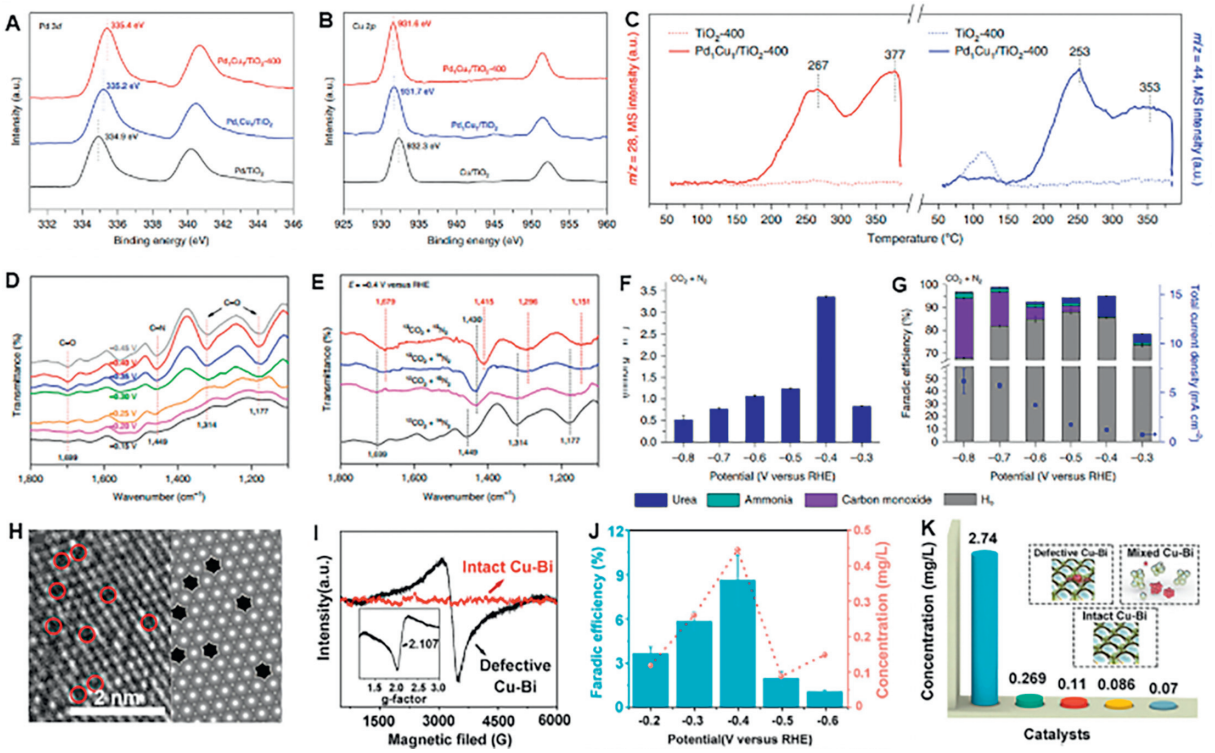

Fig. 2. Defective electrocatalysts mediated coupling of CO_2 and N_2 for urea synthesis. (A) Pd 3d XPS spectra and (B) Cu 2p XPS spectra of Cu/TiO_2, Pd_1Cu_1/TiO_2 and Pd_1Cu_1/TiO_2-400. (C) Competitive chemisorption of N_2 (red) and CO_2 (blue) on TiO_2-400 and Pd_1Cu_1/TiO_2-400. (D) Infrared signal in the range of 1100–1800 cm^{-1} under various potentials for Pd_1Cu_1/TiO_2-400 during the electrocoupling of N_2 and CO_2. (E) Isotope-labeling infrared signals in the range of 1100–1800 cm^{-1} at −0.40 V for Pd_1Cu_1/TiO_2-400 during the electrocoupling of $^{15}N_2$ and/or $^{13}CO_2$ processes. (F) Urea generation with CO_2 and N_2 as feeding gases. (G) The FE_{urea} and the total current densities for all products at various potentials. (A–G) Reproduced with permission [48]. Copyright 2020, Nature Publishing. (H) TEM image from a double-corrected spherical aberration electron microscope. (I) Comparison of EPR spectra for intact and defective Cu–Bi. (J) The concentrations and faradaic efficiencies of urea. (K) Comparison of the urea concentrations by defective Cu–Bi (blue), the mixture of Cu–Bi (green), Cu (red), intact Cu–Bi (yellow), and Bi (gray) catalysts. (H–K) Reproduced with permission [50]. Copyright 2022, Cell Press.

defective electrocatalysts mediated coupling of CO_2 and N_2 for urea synthesis are scarce, and the development of more robust defective electrocatalysts is bound to push this field forward.

3. Mechanism and role of defect in electrocatalytic synthesis of urea

3.1. Mechanism for C–N coupling of CO_2 and NO_2^-/NO_3^-

The mechanism of electrocatalytic urea synthesis from NO_2^-/NO_3^--integrated CO_2 reduction is still controversial, there are mainly four possible explanations in current reported works (Table 2). The $^*CO + ^*NH_2$ coupling mechanism observed in NO_2^-/NO_3^--integrated electrocatalytic CO_2 reduction for urea synthesis was firstly proposed by Shibata and Furuya *et al.* [33,71,72]. Recently, Liu *et al.* [39] proved the feasibility of this mechanism through density functional theory (DFT) calculations in their recent F-CNT work, and the formation of $^*CO$ and $^*NH_2$ intermediates was more favorable on F-doped C active sites ("$C–F_2$" moieties) than on C active sites (Fig. 3A). The experimental results also proved the F-CNT showed better performance toward urea synthesis than CNT, hence we deduced the introduction of V_O caused by F doping contributed to urea production. Of note, this coupling mechanism has long been controversial, and some new ideas have also put forward. For instance, Meng *et al.* [36] proposed that the V_O–ZnO porous nanosheets mediated electrocatalytic C–N formation came from the coupling of $^*NH_2$ and $^*COOH$ intermediates, which were generated from the reduction of NO_2^- and CO_2, respectively. *In situ* infrared (IR) spectra measurements indicated the $^*COOH$ peaks detected at reductive potentials under the $CO_2 + NO_2^-$ conditions were weaker than that detected at the CO_2-free conditions, and a peak attributed to C–N bond was observed, indicative of the consumption of $^*COOH$ and occurrence of C–N coupling (Fig. 3B). The experimental results indicated V_O promoted urea electrosynthesis, we therefor deduced V_O was conducive to the formation of $^*NH_2$ and $^*COOH$ intermediates. Yu's group [23,37] proposed the $^*CO_2 + ^*NO_2$ coupling mechanism using In-based materials as electrocatalysts. In their V_O–InOOH work [51], DFT calculations indicated the urea synthesis was triggered by the thermodynamically spontaneous reduction of NO_3^- to the $^*NO_2$ and the $^*CO_2NH_2$ protonation was the potential-limiting step (PLS) for the overall urea formation process (Fig. 3C). Significantly, the V_O contributed to lower the energy barrier for the protonation of the $^*CO_2NH_2$ intermediate to accelerate urea synthesis, and Bader charge analysis (Fig. 3D) and the SR-FTIR analysis (Fig. 3E) further proved this idea. In the V_O-S-IO-6 work reported by Li *et al.* [40] proposed the same C–N coupling mechanism, they illustrated the introduction of V_O significantly tuned the electronic structure around the catalytic sites to accelerate the cleavage of In–O bond in V_O-S-IO-6 adsorbed $^*CO_2NH_2$, thereby benefiting the protonation process and boosting the electrocatalytic performance of urea synthesis. Recently, Wang's group proposed the urea formation *via* a two-step coupling process. In their V_O–CeO_2 work [38], *in situ* sum frequency generation (SFG) spectroscopy analysis indicated the core of reaction mechanism was that $^*NO$ intermediate species adsorbed to V_O sites of the catalyst, and the subsequent coupling process with $^*CO$ to form $^*OCNO$ was more favorable than the hydrogenation reaction of $^*NO$, whereas the (proton-coupling electron-transfer, PCET) process of $^*NO$ tended to occur on the V_O-deficient electrocatalyst (Figs. 3F and G). DFT

Table 1
Electrocatalytic urea synthesis from N-integrated CO_2 reduction.

N source	Catalyst	FE_{urea} potential (V)	r_{urea}	FE_{urea} (%)	Electrolyte	Ref.
NO_2^-	V_O–Cu–TiO_2	−0.4	20.8 μmol/h	43.10	0.2 mol/L $KHCO_3$ + 0.02 mol/L KNO_2	[35]
	Te–Pd NCs	−1.1	/	12.20	0.1 mol/L $KHCO_3$ + 0.01 mol/L KNO_2	[2]
	V_O–ZnO	−0.79	16.56 μmol/h	23.26	0.2 mol/L $NaHCO_3$ + 0.02 mol/L $NaNO_2$	[36]
	ZnO		7.72 μmol/h	8.1		
	AuCu nanofibers	−1.55 *vs.* Ag/AgCl	3889.6 μg h^{-1} mg^{-1}	24.7	0.5 mol/L $KHCO_3$ + 0.01 mol/L KNO_2	[51]
	Co–NiO_x@GDY	−0.7	913.2 μg h^{-1} mg^{-1}	64.3	0.01 mol/L $NaNO_2$	[52]
NO_3^-	TiO_2–Nafion	−0.52	0.15 μmol/h	40.00	0.1 mol/L KNO_3	[53]
	$In(OH)_3$	−0.6	533.1 μg h^{-1} mg^{-1}	54.30	0.1 mol/L KNO_3	[23]
	V_O–InOOH	−0.5	592.5 μg h^{-1} mg^{-1}	51.00	0.1 mol/L KNO_3	[37]
	InOOH		378.4 μg h^{-1} mg^{-1}	26.3		
	B-FeNi-DASC	−1.5	20.2 mmol g^{-1} h^{-1}	17.80	0.1 mol/L $KHCO_3$ + 0.05 mol/L KNO_3	[54]
	V_O–CeO_2-750	−1.6	943.6 mg g^{-1} h^{-1}	~3.7	0.1 mol/L $KHCO_3$ + 0.05 mol/L KNO_3	[38]
	CeO_2		~350 mg g^{-1} h^{-1}	~1.1		
	F-CNT-300	−0.65	6.36 mmol g^{-1} h^{-1}	18.00	0.1 mol/L KNO_3	[39]
	CNT		~1.67 mmol g^{-1} h^{-1}	/		
	V_O-S-IO-6	−0.6	910.4 μg h^{-1} mg^{-1}	60.6	0.1 mol/L KNO_3	[40]
	Cu@Zn	−1.02	7.29 μmol cm^{-2} h^{-1}	9.28	0.2 mol/L $KHCO_3$ + 0.1 mol/L KNO_3	[55]
	Fe(a)@C–Fe_3O_4/CNTs	−0.65	1341.3 ± 112.6 μg h^{-1} mg^{-1}	16.5 ± 6.1	0.1 mol/L KNO_3	[56]
	PdCu/CBC	−0.5	763.8 ± 42.8 μg h^{-1} mg^{-1}		0.05 mol/L KNO_3	[57]
		−0.4		69.1 ± 3.8		
	$CoRuN_6$	−0.6	8.98 mmol g^{-1} h^{-1}	25.31	0.1 mol/L KNO_3	[58]
	m-Cu_2O	−1.3	29.2 mmol g^{-1} h^{-1}	9.43	0.1 mol/L $KHCO_3$ + 0.01 mol/L KNO_3	[59]
	L–Cu_1–CeO_2	−1.6	52.84 mmol g^{-1} h^{-1}	~5.4	0.1 mol/L $KHCO_3$ + 0.05 mol/L KNO_3	[60]
	MoO*x*/C	−0.6	1431.5 μg h^{-1} mg^{-1}	27.2	0.1 mol/L KNO_3	[61]
	6 Å-Cu	−0.4	7541.9 μg h^{-1} mg^{-1}	51.9	0.1 mol/L KNO_3	[62]
	CoPc-COF@TiO_2 NTs	−0.6	1205 μg h^{-1} cm^{-2}	49	0.3 mol/L $KHCO_3$ + 0.2 mol/L KNO_3	[63]
N_2	Pd_1Cu_1/TiO_2–V_O-400	−0.4	3.36 mmol g^{-1} h^{-1}	8.92	0.1 mol/L $KHCO_3$	[48]
	Pd_1Cu_1/TiO_2–V_O	−0.5	166.67 mol_{urea} mol_{Pd}^{-1} h^{-1}	22.54	0.1 mol/L $KHCO_3$	[49]
	Cu–Bi nanoalloy	−0.4	5.27×10^{11} mol s^{-1} cm^{-2}	8.7 ± 1.7	0.05 mol/L KNO_3	[50]
	Bi–$BiVO_3$	−0.4	5.91 mmol g^{-1} h^{-1}	12.55	0.1 mol/L $KHCO_3$	[64]
	$BiFeO_3$/$BiVO_4$	−0.4	4.95 mmol g^{-1} h^{-1}	17.18	0.1 mol/L $KHCO_3$	[65]
	$Ni_3(BO_3)_2$	−0.5	582.1 μg h^{-1} mg^{-1}	20.36	0.1 mol/L $KHCO_3$	[66]
	CuPc NTs	−0.6	143.47 μg h^{-1} mg^{-1}	12.99	0.1 mol/L $KHCO_3$	[67]
	MoP-(101)	−0.35	12.4 μg h^{-1} mg^{-1}	36.5	0.1 mol/L $KHCO_3$	[68]
	Cu^{III}-HHTP	−0.6	7.78 mmol g^{-1} h^{-1}	23.09	0.1 mol/L $KHCO_3$	[69]
	ZnMn–N,Cl	−0.3	4.0 mmol g^{-1} h^{-1}	63.5	0.1 mol/L $KHCO_3$	[70]

Table 2
Proposed mechanism of electrocatalytic urea synthesis from NO_2^-/NO_3^--integrated CO_2.

Mechanism		N source	Catalyst	Ref.
$^*CO + ^*NH_2$		NO_2^-	V_O–Cu–TiO_2	[35]
		NO_2^-	Te–Pd NCs	[2]
		NO_2^-	AuCu nanofibers	[51]
		NO_3^-	TiO_2–Nafion	[53]
		NO_3^-	F-CNT	[39]
		NO_3^-	Cu@Zn	[55]
		NO_3^-	Fe(a)@C-Fe_3O_4/CNTs	[56]
$^*COOH + ^*NH_2$		NO_2^-	V_O–ZnO	[36]
$^*CO_2 + ^*NO_2$		NO_2^-	Co–NiOx@GDY	[52]
		NO_3^-	$In(OH)_3$	[23]
		NO_3^-	V_O–InOOH	[37]
		NO_3^-	PdCu/CBC	[57]
		NO_3^-	V_O-S-IO-6	[40]
		NO_3^-	$CoRuN_6$	[58]
		NO_3^-	MoO*x*/C	[61]
		NO_3^-	CoPc-COF@TiO_2 NTs	[63]
Two-step coupling process	(1) $^*CO + ^*NH \rightarrow ^*NHCO$; (2) $^*NHCO + ^*NO \rightarrow ^*NHCONO$	NO_2^-	B–FeNi-DASC	[54]
		NO_2^-	V_O–CeO_2-750	[38]
	(1) $^*CO + ^*NO \rightarrow ^*ONCO$; (2) $^*ONCO + ^*NO \rightarrow ^*ONCONO$	NO_3^-	m-Cu_2O	[59]
		NO_3^-	L–Cu_1–CeO_2	[60]

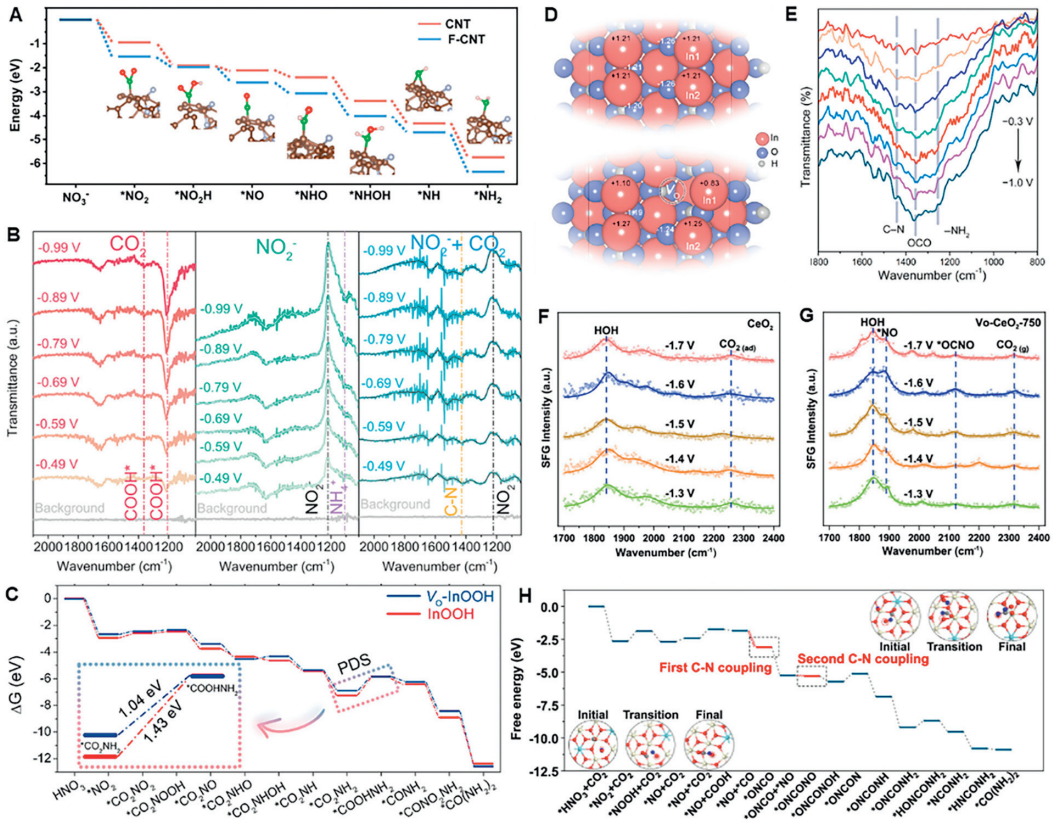

Fig. 3. *In situ* characterization and proposed coupling mechanism for electrocatalytic urea synthesis from NO_2^-/NO_3^--integrated CO_2 reduction. (A) Potential energy diagrams of NO_3^- reduction to $*NH_2$, undoped CNT and F-doped C active sites (F-CNT) are marked. C, O, H, F and N atoms are represented as brown, red, pinkish white, blue and green spheres, respectively. Reproduced with permission [39]. Copyright 2022, Elsevier Inc. (B) *In situ* ART-FTIR spectra of ZnO-V under CO_2, $NaNO_2$, and both. Reproduced with permission [36]. Copyright 2021, Cell Press. (C) Free-energy diagrams for urea production on the facets of V_O-InOOH and pristine InOOH at 0 V. (D) Bader charge analysis on V_O-InOOH and pristine InOOH. (E) Infrared signals in the range of 800−1800 cm^{-1} obtained from *operando* SR-FTIR spectroscopy measurements under various potentials (−0.3 V to −1.0 V) for V_O-InOOH during the electrocatalytic coupling of NO_3^- and CO_2. (C–E) Reproduced with permission [37]. Copyright 2021, American Chemical Society. SFG signals of intermediate species on (F) pristine CeO_2 and (G) Vo-CeO_2-750. (H) Free energy diagram of urea production on Vo-enriched CeO_2. The insets are the initial, transition, and final states of C–N coupling processes. The gray, blue, red, white, and cyan balls represent C, N, O, Ce(IV), and Ce(III) atoms, respectively; the dash circles represent oxygen vacancies. (F–H) Reproduced with permission [38]. Copyright 2022, American Chemical Society.

calculations indicate the C–N coupling was thermodynamically and kinetically favorable on Vo-enriched CeO_2, and meanwhile, a novel two-step coupling mechanism, namely, $*CO + *NO \rightarrow *ONCO$ and $*ONCO + *NO \rightarrow *ONCONO$, was proposed (Fig. 3H). In addition, another two-step coupling mechanism of $*CO + *NO \rightarrow *ONCO$; (2) $*ONCO + *NO \rightarrow *ONCONO$ was also proposed [59,60], but the related works did not involve defective electrocatalysts.

3.2. Mechanism for C–N coupling of CO_2 and N_2

N_2-integrated electrocatalytic CO_2 reduction reaction involves multistep electrochemical processes and nonelectrochemical processes, and probably share the similar C–N coupling mechanism as the co-reduction of CO_2 and NO_2^-/NO_3^-. Generally, the coupling reaction occurs through the formation of C–N bonds *via* the thermodynamically spontaneous reaction between *N=N* and CO. In the Pd_1Cu_1/TiO_2-V_O-400 work [48], DFT calculations illustrated that the key urea precursor of tower-like *NCON*, was formed *via* the reaction between *N=N* and CO in a thermodynamically and kinetically feasible way, then *NCON* was hydrogenated following a distal pathway to form urea, and the third proton-coupled electron transfer process was energy demanding and was the PLS of urea (Fig. 4A). The formation of C–N bond was proved by SR-FTIR analysis (Figs. 2E and F), but the structure of *NCON* intermediates and the role of V_O were not well identified. The same C–N coupling process was proposed by Zhang's group [64] in the Bi–$BiVO_4$ work, but *NCON* was hydrogenated in an alternating pathway rather than in a distal pathway, and the PLS was the generation of *NHCONH intermediate (Figs. 4B and C). This hypothetical *NCON* pathway for urea formation involved two N atoms bond with one C atom simultaneously, which was obviously different from the pathways in electrocatalytic co-reduction of CO_2 and NO_2^-/NO_3^-. Of note, such a dual C–N bond-forming step circumvented the formation of highly unstable formamide or carbamic acid intermediates. In the defective Cu–Bi catalyst work reported by Wu *et al.* [50], Raman signal of C–N intermediates on defective Cu–Bi immersed in both N_2 and CO_2 atmosphere was observed (Fig. 4D), and no evidence of co-reduction N_2 and CO_2 was found on contrast catalysts including Cu, Bi, mixed Cu–Bi, and intact Cu–Bi (Fig. 4E), indicating the defective Cu–Bi had the most abundant active sites to produce urea by coupling N_2 and CO_2. DFT calculations indicated the defective Cu–Bi Gibbs free energy decreased in the presence of N_2 and CO_2, while the intact Cu–Bi did not show a significant preference for *COOH ($*N_2$) and *COOH, which suggested that the defective Cu–Bi could offer important advantages over that intact Cu–Bi on coupling C–N intermediates (Fig. 4F). In addition, rate-determining step (RDS) barriers were also used to evaluate the catalytic activity. As shown in Figs. 4G and H, the RDS for the distal and alternating styles of intact Cu–Bi was from $*NN + *CO$ to *NCON* step, amounting to a barrier of 2.63 eV, and relative lower RDS barriers were posed by comparing the distal (from *NHCON to *NHHCON, 0.78 eV) and alternating (from $*NN + *CO$ to *NCON*,

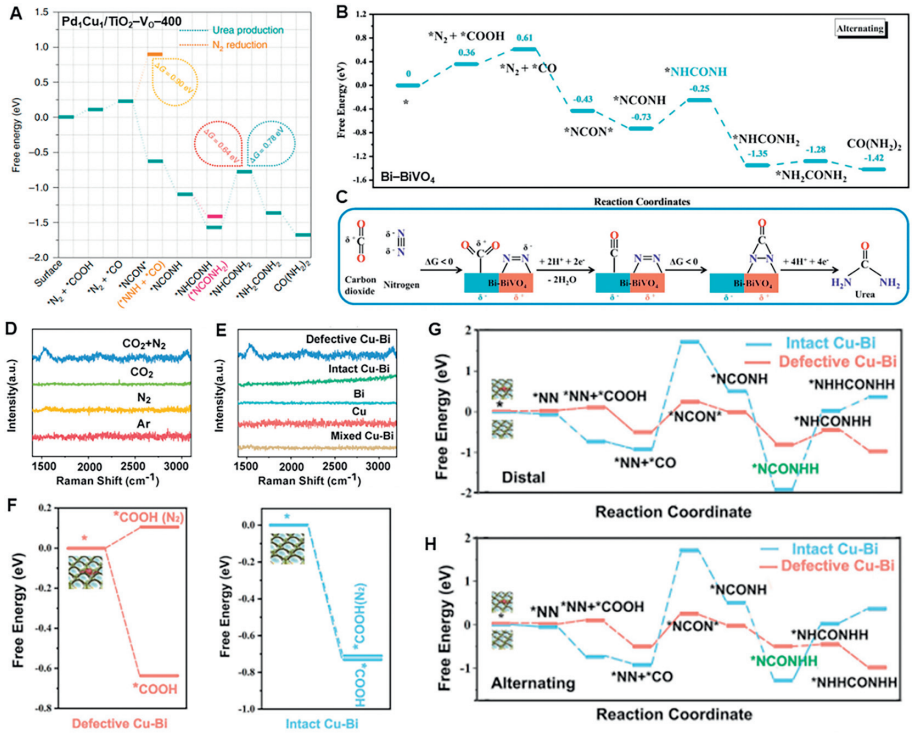

Fig. 4. *In situ* characterization and proposed coupling mechanism for Pd_1Cu_1/TiO_2-V_O-400 mediated electrocatalytic urea synthesis from N_2-integrated CO_2 reduction. (A) Free energy diagram of urea production. Reproduced with permission [48]. Copyright 2020, Nature Publishing. (B) Electrolytic urea production *via* the alternating mechanism. (C) Mechanism of the electrocatalytic urea synthesis based on synergistic effects of the Bi–$BiVO_4$ Mott–Schottky heterostructure. (B, C) Reproduced with permission [64]. Copyright 2021, Wiley-VCH. Comparison of Raman signals with different (D) feeding gases and (E) catalysts. (F) Comparison of free-energy diagram of the CO_2 reduction with and without the assistance of N_2. (G, H) Free-energy diagram of the electrolytic urea production *via* distal and alternating mechanisms. (D–H) Reproduced with permission [50]. Copyright 2022, Cell Press.

0.76 eV) styles in defective Cu–Bi. This work paved the way to further advances in designing other defective electrocatalysts for N_2 and CO_2 co-reduction operation. Subsequent works also proposed the same coupling steps as the above two works, but further investigation was still desired to verify the C–N coupling process, especially the formation of *NCON* intermediate. Recently, theoretical scientists have carried out some theoretical calculation works to help researchers to better understand the C–N coupling mechanism of N_2-integrated electrocatalytic CO_2 reduction reaction [73–76], but the role of defect was not well explored.

The mechanisms for urea synthesis from N-integrated O_2 reduction are controversial, and more detailed *in situ* characterization should be identified, especially the formation of key intermediates. Anyway, the defects are certainly proved to act the role of extra active sites to modulate the nearby active sites' electronic structure, facilitating the formation of vital intermediates and higher reaction efficiency. Further research is bound to develop more robust defect engineering strategy to improve the selectivity, FE and yield of urea synthesis.

4. Conclusions and outlooks

This minireview summarized the recent advances of defect engineered electrocatalysts in urea electrosynthesis from CO_2 and various N reactants (NO_2^-/NO_3^- and N_2). Although the works about defective engineered C–N coupling reactions toward urea synthesis were scarce, the introduction of defect was proved to be able to significantly tune the electronic structure around the catalytic sites to accelerate the formation of key intermediates, thereby benefiting the protonation process and boosting the electrocatalytic performance of urea synthesis. However, the selectivity, yield and FE of defective catalysts mediated urea production are still limited. The biggest obstacle to limiting the development of this field is the key intermediates and specific reaction path for urea production are not very well identified, which hindered the design and improvement of defective electrocatalysts.

In the future, more efforts must made to promote the development of defective engineering strategy mediated electrocatalytic urea production. Firstly, rational methods should be explored to accurately control the types of defects in electrocatalysts. Secondly, the relationship between defect type and catalytic reaction activity, and the specific role of defects in the C–N coupling reaction process should be uncovered by more robust and reliable *in situ* characterization techniques. Lastly, efficient strategies should be developed to synthesize large-scale defective catalysts and design specific reactors to realize large-scale production of urea. We sincerely hope further investigations of defect engineered electrocatalysts for building C–N bonds can be motivated by this minireview, and further achieve sustainable electrosynthesis of different types of organonitrogen compounds including urea.

Declaration of competing interest

The authors declare that they have no known competing financial interests or personal relationships that could have appeared to influence the work reported in this paper.

Acknowledgments

This work was supported by the National Natural Science Foundation of China (Nos. 22278094 and 22209029), Outstanding Youth Project of Guangdong Natural Science Foundation (No. 2020B1515020028), Guangdong Natural Science Foundation (No. 2022A1515011775), University Innovation Team Scientific Research

Project of Guangzhou Education Bureau (No. 202235246) and China Postdoctoral Science Foundation (No. 2023M730760).

References

[1] M. Jouny, J.J. Lv, T. Cheng, et al., Nat. Chem. 11 (2019) 846–851.
[2] Y. Feng, H. Yang, Y. Zhang, et al., Nano Lett. 20 (2020) 8282–8289.
[3] J.E. Kim, S. Choi, M. Balamurugan, et al., Trends Chem. 2 (2020) 1004–1019.
[4] M.T. Sabatini, L.T. Boulton, H.F. Sneddon, et al., Nat. Catal. 2 (2019) 10–17.
[5] X. Wang, Nat. Catal. 2 (2019) 98–102.
[6] M. Alfian, W.W. Purwanto, Energy Sci. Eng. 7 (2019) 292–304.
[7] M. Yamauchi, H. Saito, T. Sugimoto, et al., Coord. Chem. Rev. 472 (2022) 214773.
[8] C.Y. Lin, D. Zhang, Z. Zhao, et al., Adv. Mater. 30 (2018) 1703646.
[9] L.F.T. Novaes, J. Liu, Y. Shen, et al., Chem. Soc. Rev. 50 (2021) 7941–8002.
[10] X. Peng, L. Zeng, D. Wang, et al., Chem. Soc. Rev. 52 (2023) 2193–2217.
[11] Z. Tao, C.L. Rooney, Y. Liang, et al., J. Am. Chem. Soc. 143 (2021) 19630–19642.
[12] J. Wang, Z. Yao, L. Hao, et al., Curr. Opin. Green Sustain. 37 (2022) 100648.
[13] Z. Mei, Y. Zhou, W. Lv, et al., ACS Sustain. Chem. Eng. 10 (2022) 12477–12496.
[14] Y. Huang, R. Yang, C. Wang, et al., ACS Energy Lett. 7 (2021) 284–291.
[15] J. Li, Y. Zhang, K. Kuruvinashetti, et al., Nat. Rev. Chem. 6 (2022) 303–319.
[16] X. Fu, J. Zhang, Y. Kang, Chem. Catal. 2 (2022) 2590–2613.
[17] M. Fasihi, R. Weiss, et al., J. Appl. Energy 294 (2021) 116170.
[18] G. Qing, R. Ghazfar, S.T. Jackowski, et al., Chem. Rev. 120 (2020) 5437–5516.
[19] S. Raghunathan, T. Jaganade, U.D. Priyakumar, Biophys. Rev. 12 (2020) 65–84.
[20] L. Celleno, Dermatol. Ther. 31 (2018) e12690.
[21] Z.J. Schiffer, K. Manthiram, Joule 1 (2017) 10–14.
[22] C. Chen, N. He, S. Wang, Small Sci. 1 (2021) 2100070.
[23] C. Lv, L. Zhong, H. Liu, et al., Nat. Sustain. 4 (2021) 868–876.
[24] X. Liu, Y. Jiao, Y. Zheng, et al., Nat. Commun. 13 (2022) 5471.
[25] J.M.P. Martirez, E.A. Carter, ACS Nano 10 (2016) 2940–2949.
[26] Y. Jia, K. Jiang, H. Wang, et al., Chem 5 (2019) 1371–1397.
[27] C. Xie, D. Yan, W. Chen, et al., Mater. Today 31 (2019) 47–68.
[28] X. Yan, Y. Jia, X. Yao, Small Struct. 2 (2021) 2000067.
[29] Z. Xiao, C. Xie, Y. Wang, et al., J. Energy Chem. 53 (2021) 208–225.
[30] W. Li, D. Wang, Y. Zhang, et al., Adv. Mater. 32 (2020) 1907879.
[31] Y. Lu, L. Zhou, S. Wang, et al., Nano Res. 16 (2023) 1890–1912.
[32] M. Shibata, K. Yoshida, N. Furuya, J. Electrochem. Soc. 145 (1998) 595.
[33] M. Shibata, N. Furuya, J. Electroanal. Chem. 507 (2001) 177–184.
[34] C. Lv, J. Liu, C. Lee, et al., ACS Nano 16 (2022) 15512–15527.
[35] N. Cao, Y. Quan, A. Guan, et al., J. Colloid Interf. Sci. 577 (2020) 109–114.
[36] N. Meng, Y. Huang, Y. Liu, et al., Cell Rep. Phys. Sci. 2 (2021) 100378.
[37] C. Lv, C. Lee, L. Zhong, et al., ACS Nano 16 (2022) 8213–8222.
[38] X. Wei, X. Wen, Y. Liu, et al., J. Am. Chem. Soc. 144 (2022) 11530–11535.
[39] X. Liu, P.V. Kumar, Q. Chen, et al., Appl. Catal. B: Environ. 316 (2022) 121618.
[40] Z. Li, P. Zhou, M. Zhou, et al., Appl. Catal. B: Environ. 338 (2023) 122962.
[41] S. Zhang, M. Jin, T. Shi, et al., Angew. Chem. Int. Ed. 59 (2020) 13423–13429.
[42] D. Yao, C. Tang, L. Li, et al., Adv. Energy Mater. 10 (2020) 2001289.
[43] D.B. Kayan, F. Köleli, Appl. Catal. B: Environ. 181 (2016) 88–93.
[44] Y.E. Kim, B. Kim, W. Lee, et al., Chem. Eng. J. 413 (2021) 127448.
[45] Y. Zhang, X. Chen, W. Wang, et al., Appl. Catal. B: Environ. 310 (2022) 121346.
[46] Z. Wei, Z. Gu, Y. Zhang, et al., Appl. Catal. B: Environ. 320 (2023) 121915.
[47] H. Su, J. Jiang, N. Li, et al., Chem. Eng. J. 446 (2022) 137226.
[48] C. Chen, X. Zhu, X. Wen, et al., Nat. Chem. 12 (2020) 717–724.
[49] L. Pan, J. Wang, F. Lu, et al., Angew. Chem. 135 (2023) e202216835.
[50] W. Wu, Y. Yang, Y. Wang, et al., Chem Catal. 2 (2022) 3225–3238.
[51] S. Liu, S. Yin, Z. Wang, et al., Cell Rep. Phys. Sci. 3 (2022) 100869.
[52] D. Zhang, Y. Xue, X. Zheng, et al., Natl. Sci. Rev. 10 (2023) nwac209.
[53] D. Saravanakumar, J. Song, S. Lee, et al., ChemSusChem 10 (2017) 3999–4003.
[54] X. Zhang, X. Zhu, S. Bo, et al., Nat. Commun. 13 (2022) 5337.
[55] N. Meng, X. Ma, C. Wang, et al., ACS Nano 16 (2022) 9095–9104.
[56] J. Geng, S. Ji, M. Jin, et al., Angew. Chem. Int. Ed. 62 (2023) e202210958.
[57] S. Zhang, J. Geng, Z. Zhao, et al., EES Catal. 1 (2023) 45–53.
[58] C. Liu, H. Tong, P. Wang, et al., Appl. Catal. B: Environ. 336 (2023) 122917.
[59] M. Qiu, X. Zhu, S. Bo, et al., CCS Chem. (2023), doi:10.31635/ccschem.023.202202408.
[60] X. Wei, Y. Liu, X. Zhu, et al., Adv. Mater. 35 (2023) 2300020.
[61] M. Sun, G. Wu, J. Jiang, et al., Angew. Chem. Int. Ed. 62 (2023) e202301957.
[62] S. Shin, S. Sultan, Z.-X. Chen, et al., Energy Environ. Sci. 16 (2023) 2003–2013.
[63] N. Li, H. Gao, Z. Liu, et al., Sci. China Chem. 66 (2023) 1–8.
[64] M. Yuan, J. Chen, Y. Bai, et al., Angew. Chem. 133 (2021) 11005–11013.
[65] M. Yuan, J. Chen, Y. Bai, et al., Chem. Sci. 12 (2021) 6048–6058.
[66] M. Yuan, J. Chen, Y. Xu, et al., Energy Environ. Sci. 14 (2021) 6605–6615.
[67] J. Mukherjee, S. Paul, A. Adalder, et al., Adv. Funct. Mater. 32 (2022) 2200882.
[68] D. Jiao, Y. Dong, X. Cui, et al., J. Mater. Chem. A 11 (2023) 232–240.
[69] Y. Gao, J. Wang, Y. Yang, et al., Nano-Micro Lett. 15 (2023) 158.
[70] X. Zhang, X. Zhu, S. Bo, et al., Angew. Chem. Int. Ed. 62 (2023) e202305447.
[71] M. Shibata, K. Yoshida, N. Furuya, J. Electroanal. Chem. 387 (1995) 143–145.
[72] M. Shibata, K. Yoshida, N. Furuya, Denki Kagaku Oyobi Kogyo Butsuri Kagaku 66 (1998) 584–589.
[73] P. Roy, A. Pramanik, P. Sarkar, J. Phys. Chem. Lett. 12 (2021) 10837–10844.
[74] X. Zhu, X. Zhou, Y. Jing, et al., Nat. Commun. 12 (2021) 4080.
[75] Z. Zhang, L. Guo, J. Du, et al., New J. Chem. 46 (2022) 5278–5287.
[76] C. Zhu, Y. Geng, X. Yao, et al., Small Methods 7 (2023) 2201331.